Physics of the Earth and Planetary Interiors 234 (2014) 35–45

Contents lists available at ScienceDirect

Physics of the Earth and Planetary Interiors

journal homepage: www.elsevier.com/locate/pepi

Dynamic lithospheric response to megathrust and precursory seismicity features of megathrust

Junhyung Lee, Tae-Kyung Hong *

Yonsei University, Department of Earth System Sciences, 50 Yonsei-ro, Seodaemun-gu, Seoul 120-749, South Korea

ARTICLE INFO

Article history:
Received 28 December 2013
Received in revised form 17 June 2014
Accepted 27 June 2014
Available online 9 July 2014

Keywords:
Megathrust
Dynamic lithospheric response
Slip-dependent earthquake occurrence rate
Temporal seismicity change
Prediction of megathrust
Normal-faulting events

ABSTRACT

Temporal variations of seismic properties in inner trench regions before and after three megathrusts with magnitudes greater than or equal to 8.8 since 2004 are investigated to understand the nature of megathrust earthquakes. The seismicity was increased significantly, and the fault-type compositions changed after megathrusts. The seismicity displays characteristic fault-type-dependent distribution on rupture planes. The postseismic thrustal events were populated around the down-dip rupture margins due to the concentration of shear stress after coseismic ruptures. Normal-faulting earthquakes increased after the megathrusts particularly in shallow-depth regions with large slips, which may be associated with lithospheric rebound and development of splay faults. The earthquake occurrence rate (*b* value) displays a characteristic slip-dependent feature. The earthquake occurrence rates decrease with the slip amount of forthcoming megathrust, which may be caused by continuous accumulation of plate-driven stress and tectonic loading around the future rupture planes on the slab surface. The slip dependency of earthquake occurrence rates is enhanced with time until the occurrence of megathrust. The level of seismicity after megathrust is inversely proportional to that before megathrust, yielding comparable average seismicity over the rupture zone. It was also observed that the dynamic lithospheric response is highly correlated with slip distribution on the rupture plane. The tension axes of the normal-faulting earthquakes for 100 days after the Tohoku-Oki earthquake focus to an apparent pole, suggesting a radial viscoelastic deformation of lithosphere. The temporal changes of slip-dependent *b* values fit well with an exponential function, suggesting an exponential increase of normal stress on the locked region with time until the occurrence of the megathrust. This observation suggests that the temporal variation of slip-dependent *b* values may be useful for prediction of forthcoming megathrusts at least several tens years beforehand.

1. Introduction

Great earthquakes cause devastating damages. Understanding the nature of megathrusts is crucial for seismic hazard mitigation. In particular, understanding the source physics may aid in predicting forthcoming megathrusts. Several precursory features before a large events have been reported. One prominent feature is the observation of seismic quiescence before large earthquake (Wyss and Martirosyan, 1998; Enescu and Ito, 2001). Another feature is the observation of decreasing earthquake occurrence rates (*b* values) before megathrust (e.g., Nuannin et al., 2005; Moreno et al., 2010; Nanjo et al., 2012; Nuannin et al., 2012). The *b*-value variation is associated with locking on the slab surface (Ghosh et al., 2008). Such interplate coupling has been well recognized in various subduction zones (e.g., Nishimura et al., 2004).

The deficiency of large events can be judged properly with long-time seismicity records, which is difficult to achieve in regions with poor seismic monitoring systems. In addition, the *b* value analysis suggests only the possibility of occurrence of large events (e.g., Nanjo et al., 2012), However, prediction of precise occurrence time and size of forthcoming events remains unsuccessful. There have been other studies based on seismic and geophysical properties that presented possible applications to earthquake prediction (Abercrombie and Mori, 1996; Lu et al., 1999; Arabelos et al., 2001; Song and Simons, 2003). However, these features have not been observed consistently.

Seismic features after large events were also found to be changed. It has been reported that normal-faulting events increase significantly in the outer rise and inner-trench regions after large events (e.g., Asano et al., 2011; Obana et al., 2012), which is a unique postseismic feature associated with dynamic lithospheric response to a large earthquake. The lithospheric responses appear to be controlled by locking and accumulated stress on the slab

* Corresponding author.
E-mail address: tkhong@yonsei.ac.kr (T.-K. Hong).

http://dx.doi.org/10.1016/j.pepi.2014.06.012
0031-9201/

surface, which is not fully understood. The interplate coupling and lithospheric rebound are also poorly known. Thus, the properties of postseismic normal-faulting events provide information on the locking process on the slab surface.

There have been seven earthquakes with magnitudes greater than or equal to 8.8 since 1900 that have been recorded instrumentally. The 26 December 2004 M9.1 Sumatra–Andaman earthquake is the first great earthquake since the 1964 great Alaska earthquake. Two great earthquakes followed the Sumatra–Andaman earthquake (the 27 February 2010 M8.8 Maule earthquake, and the 11 March 2011 M9.0 Tohoku-Oki earthquake). These great earthquakes occurred at active convergent margins where significant tectonic stresses had been accumulating for hundreds or thousands of years (e.g., Kanamori, 1986; Minoura et al., 2001; Beavan et al., 2010).

In this study, we investigate the seismicity properties, including earthquake occurrence rate and fault-type composition, before and after the three megathrusts since 2000. The source properties and mechanical response of the lithosphere to the megathrust and the temporal variation of slip-dependent b values are investigated. We finally discuss the way how to predict a forthcoming megathrust based on the temporal variation of slip-dependent b values.

2. Events and data

The 26 December 2004 M9.1 Sumatra–Andaman earthquake is the largest event since the 1964 M9.2 Alaska earthquake. The Sumatra–Andaman earthquake ruptured unilaterally, which is similar to the 1952 M9.0 Kamchatka, the 1960 M9.5 Chile, and the 1964 M9.2 Alaska earthquakes (Ammon et al., 2005). The rupture plane extended over 1200 km along the trench. The Sumatra–Andaman earthquake occurred along the subduction zone between the Indo-Australian plate and Sunda plate (e.g., Tanioka et al., 2006) (Fig. 1). The plate convergence speed is 42 mm/year (e.g., Newcomb and McCann, 1987; Ide, 2013).

The 27 February 2010 M8.8 Maule earthquake occurred in the subduction zone between the Nazca plate and the South American plate where the plate convergence speed is as high as 80 mm/year (e.g., Angermann et al., 1999; Ide, 2013). The Maule earthquake ruptured bilaterally with two major slip patches (Delouis et al., 2010; Pollitz et al., 2011).

The 11 March 2011 M9.0 Tohoku-Oki earthquake occurred on the convergence margin between the Pacific plate and the Okhotsk plate where the convergence speed is as high as 91 mm/year (e.g., Seno and Sakurai, 1996; Apel et al., 2006). The rupture plane of the Tohoku-Oki earthquake extended ~440 km long along the Japan trench and was ~180 km wide in the trench normal direction along the slab interface (e.g., Yagi and Fukahata, 2011).

The peak coseismic slips on the rupture planes were observed to be ~20 m for the Sumatra–Andaman earthquake (Ji, 2005; Vigny et al., 2005), ~15 m for the Maule earthquake (Hayes, 2010; Lay et al., 2010), and ~50 m for the Tohoku-Oki earthquake (Yagi and Fukahata, 2011) (Fig. 1). The slips generally decrease with depth. The coseismic slips are different among the megathrusts, which may be associated with differences in interplate coupling and rupture processes (e.g., Kanamori, 1986; Lay et al., 1989). It is also noteworthy that postseismic slips occurred after the dynamic ruptures (e.g., Ozawa et al., 2011). The great earthquakes have long source durations, large slips and many normal faulting events in inner-trench regions, which display the features of tsunami earthquakes (Kanamori, 1972; McKenzie and Jackson, 2012).

Dynamic ruptures accompany lithospheric deformation, which causes crustal uplift or subsidence (Fig. 2(a)). The vertical displacements on the seafloor were −2 to 6 m in the Sumatra–Andaman earthquake region (Hoechner et al., 2008), −0.8 to 3.9 m in the Maule earthquake region (Moreno et al., 2012), and −5.3 to 14.3 m in the Tohoku-Oki earthquake region (Keliang and Jin, 2011). It is intriguing to note that the vertical displacements in the Tohoku-Oki earthquake region are different between the northern and southern source regions with comparable slip amounts.

We collected event information and focal mechanism solutions for earthquakes with magnitudes greater than 5.0 in the Sumatra–Andaman earthquake region and the Maule earthquake region between 2000 and 2013 from the Global Centroid Moment Tensor (CMT) catalog (Fig. 1). Event information of earthquakes around the Tohoku-Oki earthquake region since 1991 was collected from the Full Range Seismograph Network (F-net) and Japan Meteorological Agency (JMA) catalogues.

3. Methods and process

The type of faulting can be identified from analysis based on compressional (P), tensional (T), and null (B) axes of focal mechanism solutions (Frohlich, 1992). The P, T, and B axes are three orthogonal axes that are given by (Aki and Richards, 1980; Gasperini and Vannucci, 2003):

$$\begin{aligned}\hat{\mathbf{p}}_i &= \frac{\hat{\mathbf{n}}_i - \hat{\mathbf{d}}_i}{\sqrt{2}},\\ \hat{\mathbf{t}}_i &= \frac{\hat{\mathbf{n}}_i + \hat{\mathbf{d}}_i}{\sqrt{2}},\\ \hat{\mathbf{b}}_i &= \hat{\mathbf{e}}_{ijk}\hat{\mathbf{n}}_j\hat{\mathbf{d}}_k\end{aligned} \tag{1}$$

where $\hat{\mathbf{p}}$ is the unit P-axis vector, $\hat{\mathbf{t}}$ is the unit T-axis vector, $\hat{\mathbf{b}}$ is the unit B-axis vector, $\hat{\mathbf{n}}$ is the unit vector normal to the fault plane, $\hat{\mathbf{d}}$ is the unit slip vector, and $\hat{\mathbf{e}}$ is the unit azimuth vector.

Earthquakes with B-axis dip angles greater than 60° are defined to be strike-slip events, those with P-axis dip angles greater than 60° are normal-faulting events, and those with T-axis dip angles greater than 50° are thrustal events. Events satisfying none of these criteria are classified to have odd mechanisms that are composed of multiple source mechanisms (Frohlich, 1992).

The minimum magnitude, $M_{\min}$, of the earthquake catalog is estimated to ensure the completeness of records (Ogata and Katsura, 1993; Wiemer and Wyss, 2000; Woessner and Wiemer, 2005). The minimum magnitude is estimated using the Gutenberg-Richter magnitude-frequency relationship:

$$\log N = a - b \cdot M, \tag{2}$$

where M is the magnitude, N is the number of earthquakes with magnitudes greater than or equal to M, and a and b are constants. The constants a and b are estimated using the maximum likelihood estimation (MLE) method (Wiemer and Wyss, 2000). The b value varies by region and time, and the global average b value is ~1.0 (Wesnousky, 1994; Stein and Wysession, 2003; Schorlemmer and Wiemer, 2005; Nuannin et al., 2012).

Seismic properties may respond to the stress field that accumulates in the locked areas on the slab surface. As the rupture planes of megathrusts develop in shallow inner-trench regions, the seismic properties in the inner-trench regions may reflect the source physics. We investigate the spatial and temporal characteristics of seismicity in the inner-trench regions before and after megathrusts. The inner-trench region is segmented into three zones along subducting slabs beginning from the trench axes (zones I, II and III).

Zone I covers the shallow inner-trench region around the trench axis. Zone II covers the intermediate-depth rupture area, and zone III represents the lowermost marginal rupture area. We exclude the outer rise regions in the analysis in order to constrain only the lithospheric response around the epicenters of megathrusts.

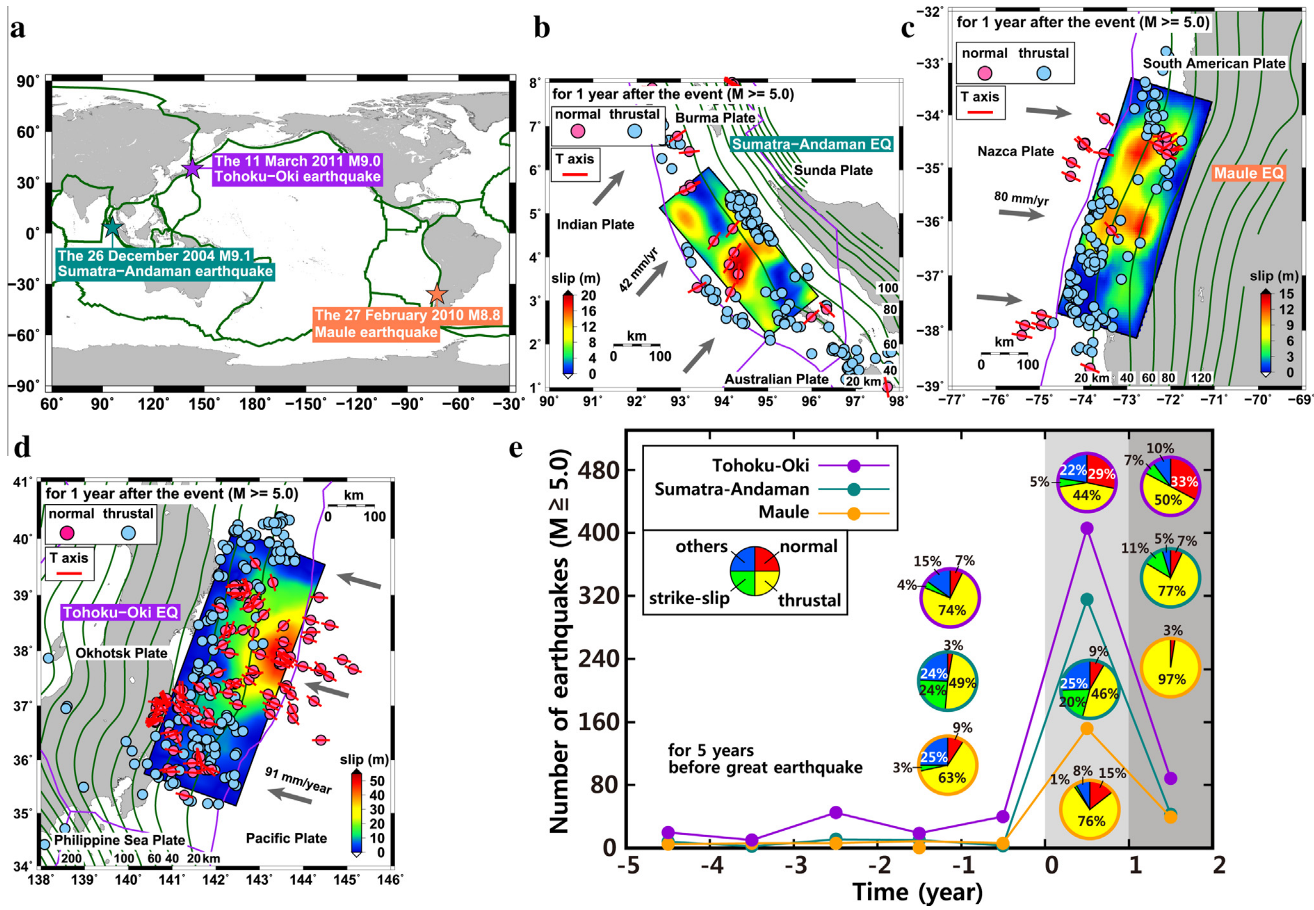

Fig. 1. (a) Map of megathrusts with magnitudes greater than or equal to 8.8 since 2000. Seismicity of earthquakes after (b) the 26 December 2004 M9.1 Sumatra–Andaman earthquake, (c) the 27 February 2010 M8.8 Maule earthquake, and (d) the 11 March 2011 M9.0 Tohoku-Oki earthquake. Slip models (Ji, 2005; Hayes, 2010; Yagi and Fukahata, 2011) and plate speeds (Newcomb and McCann, 1987; Angermann et al., 1999; Seno and Sakurai, 1996; Ide, 2013) are presented on the maps. The plate boundaries and iso-depth contours for slab surfaces are presented with solid lines (Bird, 2003; Hayes et al., 2012). Aftershocks with magnitudes greater than or equal to 5 over 1 year are presented. The tension-axis directions (red bars) are marked on the epicenters of normal-faulting events. (e) Faulting-type composition of earthquakes before and after megathrusts. The amounts of normal-faulting events increased after the megathrusts, which is particularly strong in the Tohoku-Oki earthquake region.

Each zone has a size of $90 \times 100 \times 25$ km^3 (Fig. 3(a)). The three zones take 225 km in the trench-normal direction and 65 km in the vertical direction. The shallow source region (i.e., zone I) of the Tohoku-Oki earthquake is divided into 21 subregions for investigation of along-trench variations in seismicity properties (L1 to L21 in Fig. 2 (a)). The relationships among seismicity, stress field, slip amount, and coseismic surface deformation are determined for the source region.

4. Faulting-type compositions before and after megathrusts

We analyze the faulting-type compositions in the source regions with a size of 8° in longitude and 7° latitude before and after the three megathrusts (Fig. 1). The ambient stress fields before megathrusts are dominated by compressional stress induced by convergence at the plate margins, incurring thrustal earthquakes (Fig. 2(b)). The compressional axes determined from the fault-plane solutions are naturally parallel with the plate convergence directions (Fig. 2(c)). Seismicity increased abruptly after the megathrusts, and then decreased gradually with time. The normal-faulting events occurring after megathrusts display various tension-axis directions (Fig. 1).

The number of earthquakes with magnitudes greater than 5.0 over the 5 years before the Sumatra–Andaman earthquake is 34, of which 3% (1 event) are normal-faulting earthquakes, 49% (16 events) are thrustal earthquakes, and 24% (8 events) are strike-slip earthquakes. The number of earthquakes for 1 year after the Sumatra–Andaman earthquake is 315, of which 9% (27 events) are normal-faulting earthquakes, 46% (144 events) are thrustal earthquakes, and 20% (64 events) are strike-slip earthquakes.

For the Maule earthquake region, 32 earthquakes with magnitudes greater than 5.0 occurred over the 5 years before the megathrust. The earthquakes are composed of 9% (3 events) normal-faulting events, 63% (20 events) thrustal events, and 3% (1 events) strike-slip events. The number of earthquakes for 1 year after the Maule earthquake is 152, of which 15% (22 events) are normal-faulting earthquakes, 76% (116 events) are thrustal earthquakes, and 1% (2 events) are strike-slip earthquakes.

We observe 134 earthquakes with magnitudes greater than 5.0 over the 5 years before the Tohoku-Oki earthquake. The earthquakes are composed of 7% (10 events) normal-faulting events, 74% (99 events) thrustal events, and 4% (5 events) strike-slip events. The number of earthquakes for 1 year after the megathrust is 406, of which 29% (116 events) are normal-faulting earthquakes, 44% (179 events) are thrustal earthquakes, and 5% (20 events) are strike-slip earthquakes.

These three great earthquakes share similar features in fault-type compositions and event distribution. Normal-faulting earthquakes are clustered in large slip regions, and thrustal earthquakes are populated outside the large-slip regions (Fig. 1(b–d)). In addition, the numbers of normal-faulting events

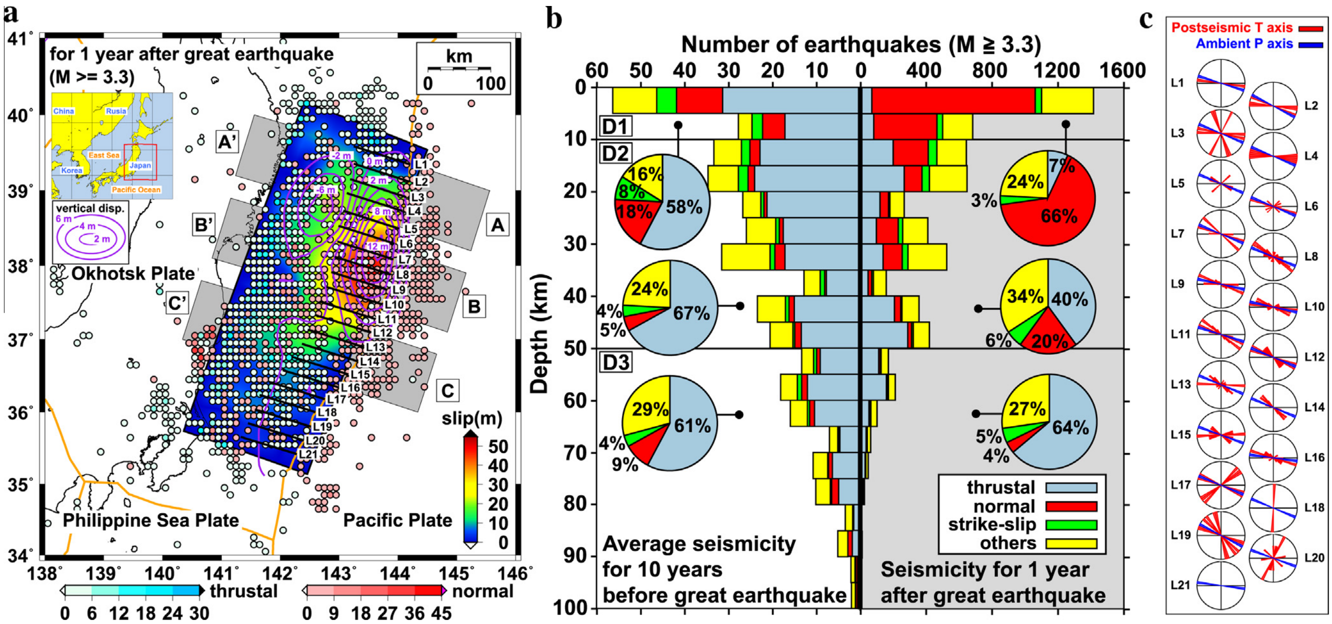

Fig. 2. (a) Seismicity of aftershocks with magnitudes greater than or equal to 3.3 after the Tohoku-Oki earthquake. The Tohoku-Oki rupture area is divided into 21 subregions (L1 to L21) for the investigation of seismicity properties. The vertical uplifts and subsidences on the Earth's surface (Hisashi, personal communication, 2013) are presented with contours. (b) Distribution of focal depths of events. The compositions of faulting type for three depth ranges are presented. The normal-faulting events are dominant at shallow depths. (c) A comparison of tensional-axis directions from normal-faulting events after the megathrust with compressional-axis directions from thrustal events before the megathrust for L1 to L21. The tensional-axis directions deviate from the ambient compressional-axis directions.

appear to be proportional to the peak slip amounts. The Tohoku-Oki earthquake has the largest peak slip (~50 m) among the great earthquakes, and presents the largest number of normal-faulting events. On the other hand, the smallest peak-slip earthquake, Maule earthquake, displays the smallest number of normal-faulting events.

Thrustal earthquakes were dominant before the megathrusts, while normal-faulting events increased after the megathrusts. This suggests that the lithospheres experienced similar deformation for accumulating stress and outburst-release of stress. These observations may allow us to infer the detailed properties of lithospheric responses to megathrust based on an analysis of seismicity in a representative megathrust region with dense seismic networks.

A dense seismic network is available in the Japanese islands, which allows for an earthquake catalog of the Tohoku-Oki region to be complete up to magnitude 3.3. The number of earthquakes with magnitudes greater than 3.3 for 5 years before the Tohoku-Oki earthquake is 1934, of which normal-faulting events comprise 9% (174 events), thrustal events comprise 60% (1170 events), and strike-slip events comprise 6% (160 events). The number of earthquakes increase to 6188 over the 1 year following the megathrust, of which 64% (2115 events) are normal-faulting events, 31% (1936 events) are thrustal faulting events, and 5% (296 events) strike-slip events. The composition of normal-faulting events is much higher in low magnitudes than in high magnitudes. This observation suggests that the earthquake occurrence rates change by faulting type, and normal-faulting events are particularly abundant among small- and moderate-sized events (Asano et al., 2011).

5. Fault-type-dependent seismicity features

The occurrence rate of normal-faulting events increased after megathrusts in all regions. The number of normal-faulting earthquakes is anti-correlated with the number of thrustal earthquakes. However, the compositions and occurrence rates of normal-faulting earthquakes are found to be different by region. Normal-faulting earthquakes compose 9–29% of the events that occurred in the first year after megathrusts. The occurrence rates of normal-faulting events in the Sumatra–Andaman and Maule regions returned to their usual rates in one year after great earthquakes. On the other hand, the Tohoku-Oki region displays abundant normal-faulting events in the second year, comprising 33% of observed events. It is intriguing to note that the number of strike-slip events was also increased in the Sumatra–Andaman earthquake region after the megathrust.

Normal-faulting earthquakes increased at depths less than 50 km, with most occurring at depths less than 10 km where slip amounts are large (Fig. 2(b)). Shallow-focus normal-faulting earthquakes are clustered in the regions with large slips. The normal-faulting events appear to be associated with the development of splay faults at shallow depths (Conin et al., 2012; Cubas et al., 2013). These splay faults may develop as a consequence of stress-field change due to depth-dependent deformation of the lithosphere after a megathrust (e.g., Asano et al., 2011; Shinohara et al., 2012). It has been suggested that the local stress field is affected by coseismic strain release and gravitational potential energy (McKenzie and Jackson, 2012). The observation implies that the faulting-type composition of each region is highly correlated with the slip amount.

The tension axes of post-megathrust normal-faulting events over the rupture surfaces display epicentral-location-dependent directions in all megathrust regions. It is observed that the tension axes are oriented outward from the peak-slip locations (Fig. 1). The seismicity compositions and tension-axis features suggest that the three megathrusts share similar lithospheric responses.

Vertical variations in seismicity and lithospheric responses along the slab surface is investigated for the Tohoku-Oki earthquake. One-year seismicity after the Tohoku-Oki earthquake is presented for three cross-sections (AA′, BB′, and CC′ in Fig. 3). Cross-section BB′ lies across the region of peak slip. Cross-sections AA′ and CC′ are placed across adjacent regions with mild slips. The zone I regions of all cross-sections show a high population of normal-faulting earthquakes and low population of thrustal earthquakes. Zone III of cross-section BB′ presents the highest

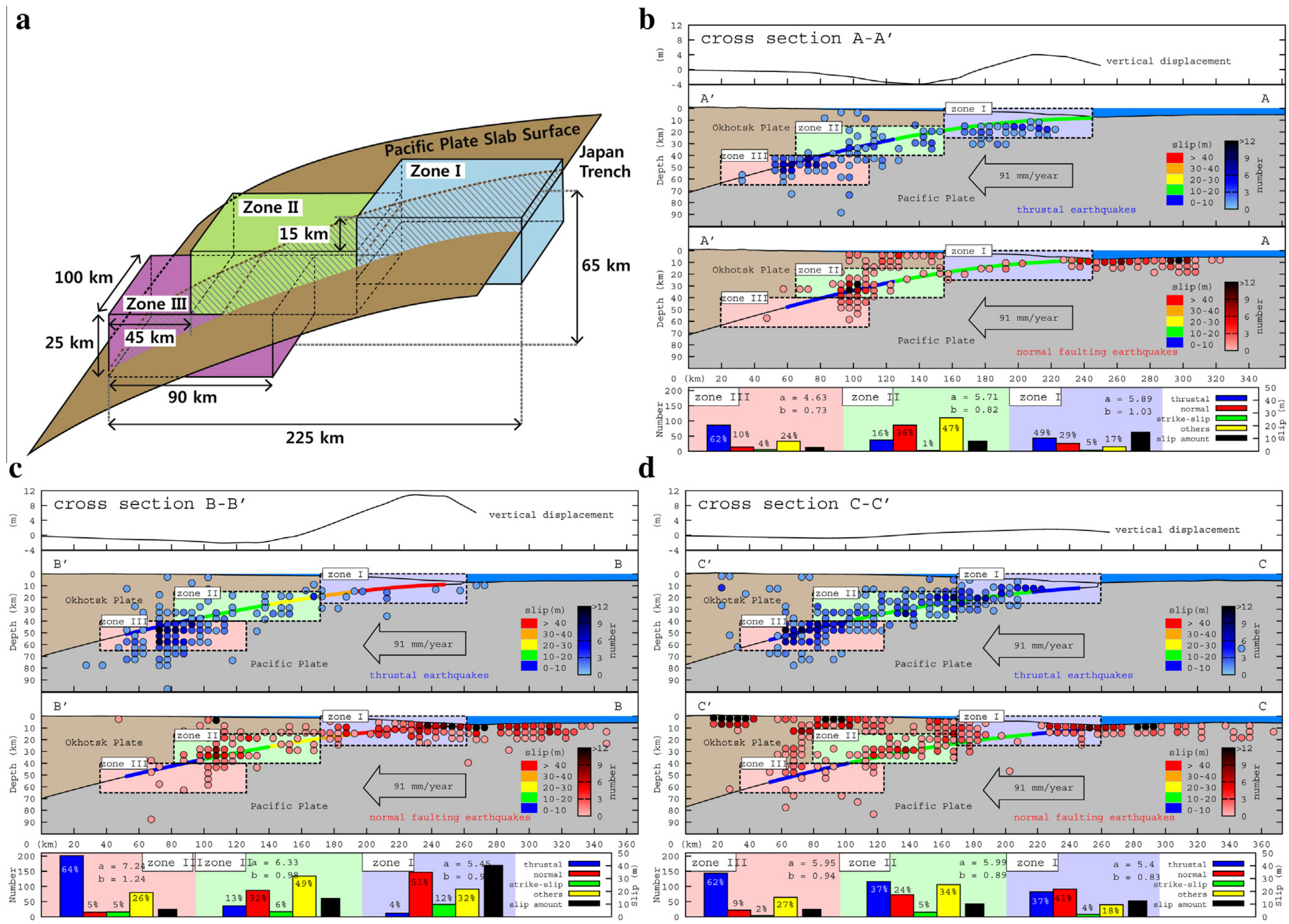

Fig. 3. Seismicity along three cross-sections in the Tohoku-Oki region (A–A′, B–B′, and C–C′ in Fig. 2(a)): (a) zonation model, (b) cross-section A–A′, (c) cross-section B–B′, and (d) cross-section C–C′. The three zones (zones I, II, and III) with a uniform size are designated along the subducting slab, starting from the trench-axis. The seismicity densities of thrustal and normal-faulting events are presented along with vertical displacements on the seafloor. The slip amounts on the rupture plane are presented along the slab boundaries. The seismicity properties (a and b values) are presented for each zone. The amount of normal-faulting events is large in zone I, and thrustal earthquakes are dominant in zone III.

seismicity, which may be because the accumulated stress in the down-dip margin of the rupture plane was not released sufficiently during coseismic slips.

The increase in seismicity after megathrust may be due to strain release associated with coseismic and postseismic lithospheric deformation (Ozawa et al., 2011). The increase in normal-faulting events suggests the prevalence of horizontal tensile stress in the shallow source region after megathrust. The relative population of thrustal earthquakes appears to increase with depth. Thrustal earthquakes are particularly clustered around the down-dip rupture edges in all three megathrust regions, which may be associated with accumulation of additional stress released from locked regions.

The one-year seismicity after the Tohoku-Oki earthquake hardly presents a fault-type-dependent b-value variation, which is different from the typical fault-type-dependent b-value variation in global seismicity (Narteau et al., 2009). Thrustal earthquakes are dominant in zone III regions of all cross-sections where the b values vary between 0.73 and 1.24 (Fig. 3). The composition of normal-faulting events is high in zone I where the b values range between 0.83 and 1.03. The seismicity in zone II is mixed with normal-faulting and thrustal events, and the b values are between 0.82 and 0.98. The differences in fault-type compositions and b values may be associated with coseismic and postseismic lithospheric deformations that cause temporal variations in the stress field of the lithosphere.

6. Relationship between aftershocks and slips

In the Tohoku-Oki earthquake region, large uplifts are observed in the seafloor above the locations of large slips (Figs. 2(a), 3(b)). Generally, the seafloor displacement is inversely proportional to the distance from the region with the largest slip amount. Seafloor subsidences are observed behind the regions with uplifts in the landward direction (Fig. 2(a)).

The number of aftershock events is the largest in the region with the peak slip amount. Also, the number of normal-faulting events is observed to be proportional to the slip amount (Figs. 4(a), 3). However, the proportionalities are different between the northern and southern regions. The northern region shows larger seafloor displacements and fewer events than the southern region with the same slip amounts. This observation suggests that the seafloor displacements are not affected only by the slip amounts, but also by the medium properties, such as geology, elasticity, and accumulated stress.

These features may suggest that the release of the stress accumulated along slab surface during the locking process before the megathrust depend on the elastic properties of the medium. The accumulated stress in the northern region might be released more effectively than that in the southern region during coseismic lithospheric rebound. The unleased stress appears to trigger more normal-faulting events in the southern region than the northern

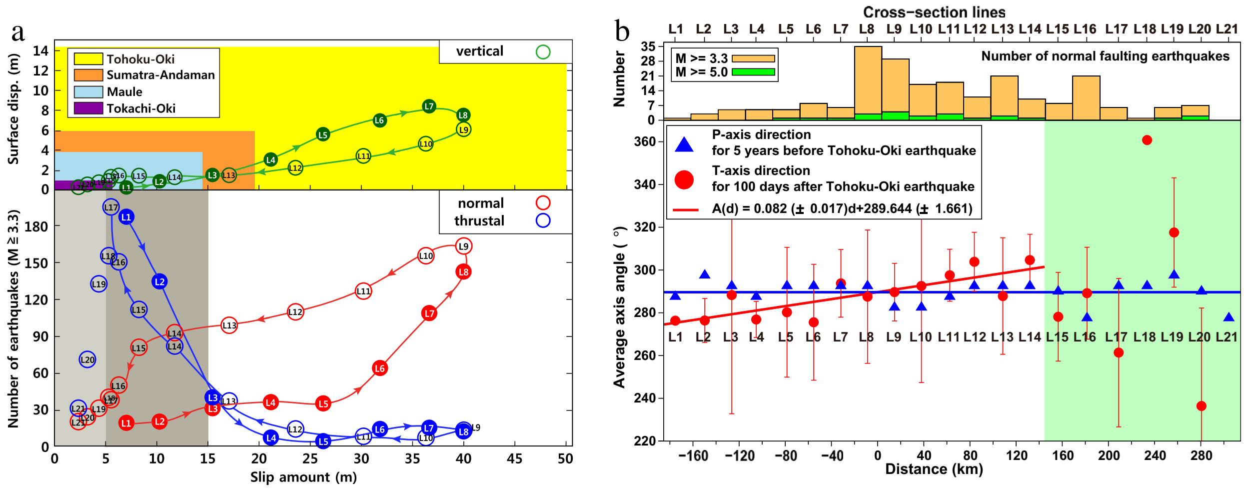

Fig. 4. (a) Numbers of thrustal and normal-faulting events, and vertical surface displacements as a function of slip amount for the 21 subregions (L1 to L21) in the Tohoku-Oki earthquake region. The ranges of vertical surface displacements (Hoechner et al., 2008; Moreno et al., 2010; Keliang and Jin, 2011) are presented with different colors by source region. The numbers of normal-faulting events are inversely proportional to those of thrustal events in regions with slip amounts larger than 5 m. The numbers of normal-faulting events are larger than those of thrustal events in regions with slips greater than 15 m. The ranges of slip amounts and vertical surface displacements of major megathrusts including the 26 September 2003 M8.0 Tokachi-Oki earthquake are indicated with colors (Mikada et al., 2006). (b) Apparent variation in tensional-axis directions of normal-faulting events, and the numbers of events for subregions L1 to L21. The tensional-axis directions at cross-sections L1 to L14 deviate from the ambient compression-axis direction. (For interpretation of the references to color in this figure legend, the reader is referred to the web version of this article.)

region. It is intriguing to note that the northern region coincides with the slow slip event region before the megathrust (Ito et al., 2013). The slow slip events in the northern region consume the energy stored in the lithosphere, making the lithosphere deformed efficiently. On the other hand, the unconsumed energy in the southern region yields a relative increase in aftershocks with subsequent delayed faulting (cf., Heki et al., 1997).

The number of normal-faulting events is anti-correlated with the number of thrustal events (Figs. 4(a), 3). The number of normal-faulting events is greater than that of thrustal events when the slip amount is greater than ~15 m (Fig. 4(a)). However, the anti-correlation relationship between normal-faulting and thrustal events is not apparent in regions with slip amounts less than ~5 m.

The ranges of vertical surface displacements and slip amounts of three megathrusts are presented in Fig. 4(a). The Tohoku-Oki earthquake displays a large peak-slip amount and vertical surface displacement compared with the other megathrusts. Megathrusts with smaller slips (i.e., Sumatra–Andaman earthquake and Maule earthquake) have fewer normal-faulting events (Fig. 1(e)). The observation of normal-faulting events in the three megathrust regions suggests that there appears to be a minimum slip amount (or a minimum vertical surface displacement) required to produce normal-faulting earthquakes.

The vertical uplifts in the northern regions of Tohoku-Oki earthquake are larger than those in the southern regions (Fig. 4(a)). The northern regions have larger vertical uplifts, but fewer normal-faulting events compared to the southern regions. Thus, the slip amount on the rupture plane and vertical surface displacement appear to be important parameters for excitation of normal-faulting earthquakes.

7. Temporal variation of ambient stress field

The compressional (P) and tensional (T) axes directions before and after the Tohoku-Oki earthquake are estimated from the focal mechanism solutions of the events. The P-axis directions for thrustal earthquakes on 21 cross-sections (L1–L21) for 5 years prior to the Tohoku-Oki earthquake are found to be 277.5°–297.5°, which

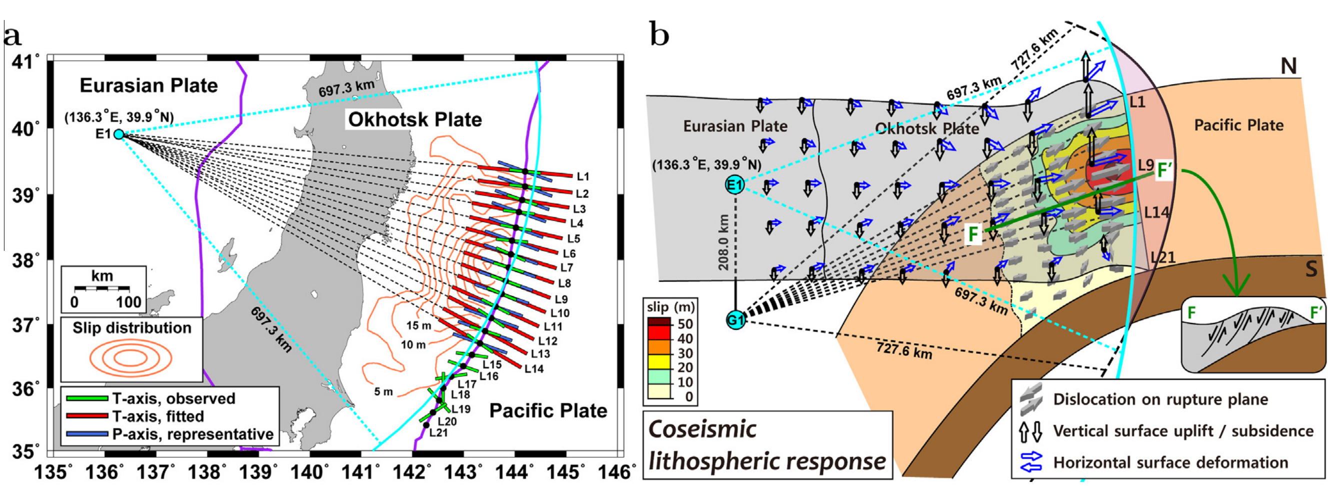

Fig. 5. (a) Apparent tensional-axis directions from normal-faulting events: the tensional axes are directed to an apparent pole in the backarc offshore region. (b) A coseismic lithospheric rebound model. The rupture along the slab surface causes coseismic lithospheric deformation. Large uplifts are observed in the seafloor above the slab surface with large slips where splay faults subsequently develop. Large subsidences are observed in the forearc regions between the inland and large-slip regions.

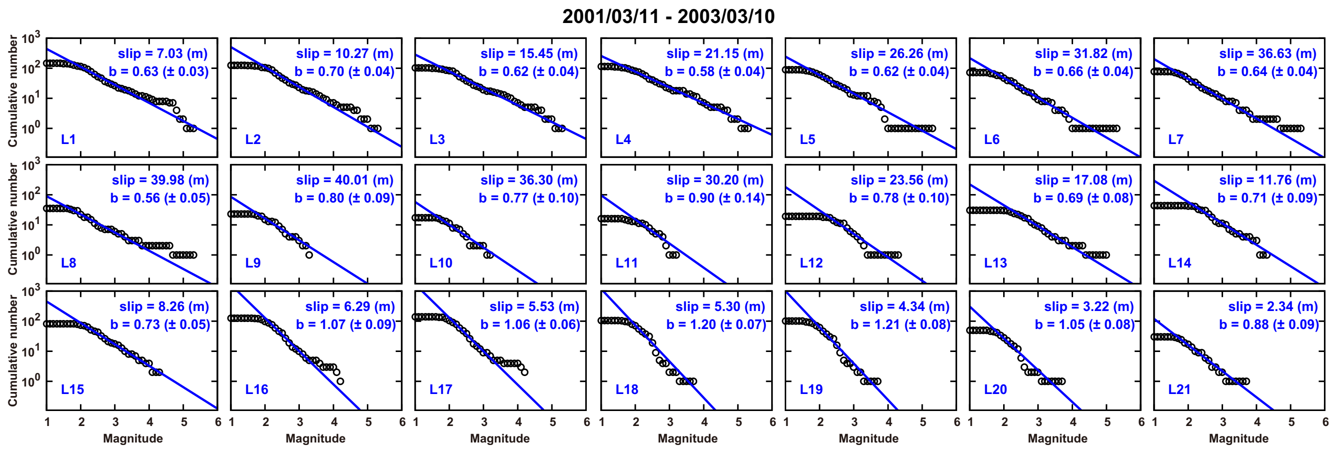

Fig. 6. Example of b value measurement for seismicity in the period of 11 March 2001 to 10 March 2003. The b values generally decrease with slip amount.

are consistent with the plate-convergence directions on the Japan trench (Fig. 2(c)). The T-axis directions estimated from the normal-faulting earthquakes during 100 days after the Tohoku-Oki earthquake are observed to vary from 180.8° to 317.5° in L1 to L21 along the trench. When we limit the region from L1 to L14, the T-axis directions display a consistent increase by location from 275.6° to 304.6° (Fig. 4(b)).

The least-squares line for the observed T-axis directions is given by

$$A(d) = 0.082(\pm 0.017)\ d + 289.644(\pm 1.661), \tag{3}$$

where $A(d)$ is the tension-axis direction at distance d. The location of $d = 0$ is placed between L8 and L9, which approximately coincides with the peak-slip location. The A-intercept (289.644°) agrees with the average P-axis direction before the megathrusts. The fitted line displays that the T axes deviate from the plate convergence direction in a consistent manner. This feature suggests that the T-axis directions are dependent on the relative locations of the events with respect to the peak-slip location. Similar variations of T-axis directions are observed in the Sumatra–Andaman and Maule earthquake regions (see Fig. 1(b)(c)).

8. Dynamic response of lithosphere

A large rupture on the slab surface causes coseismic lithospheric rebound, accompanied by regional seafloor uplift and subsidence (Fig. 3). The uplift generally appears to be proportional to the slip amount on the slab surface. The lithospheric rebound in the accretionary wedge of overriding plate causes viscoelastic relaxation of medium, incurring long-term prevalence of tensional field. The preseismic stress field is recovered slowly with time. The viscoelastic relaxation of medium and transitional stress field cause

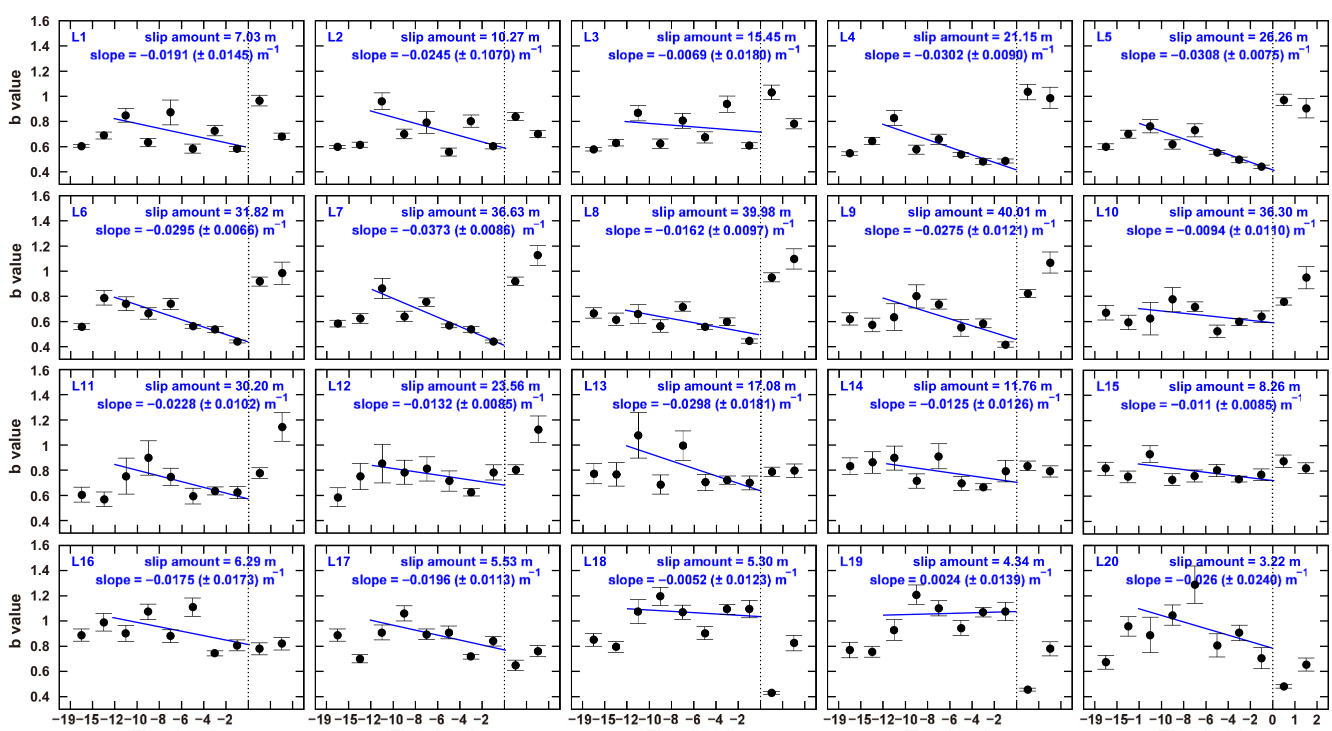

Fig. 7. Temporal variations of b values for cross-sections L1 to L20. Large-slip regions generally display large decreasing rates. The temporal b-value decreases are not significant in some regions with large slip amounts, reflecting the influence of time-dependent factors.

postseismic lithospheric deformation. Normal-faulting aftershocks appear to occur at shallow depths as a result of subsequent development of splay faults in the accretionary wedge during the coseismic and postseismic lithospheric deformation (Fig. 5). Normal-faulting earthquakes are clustered in the regions with large uplifts and subsidences (zones I and II in Fig. 3). The magnitudes of uplifts are larger than those of subsidences, which is consistent with the spatial distribution of normal-faulting events.

The T-axis directions of normal-faulting events are associated with postseismic lithospheric deformation. The T axes of normal-faulting events over 100 days following the Tohoku-Oki earthquake are presented in Fig. 4(b). The *T* axes between L1 and L14 (275.6°–304.6°) display linear deviations from the reference P-axis direction as a function of distance from the cross-section L9 that lies across the peak-slip region (Fig. 4(b)). This observation is consistent with the stress field in the upper crust after the Tohoku-Oki earthquake (Lin et al., 2013). The northern cross-sections (L1–L8) display negative angle deviations, while the southern cross-sections (L10–14) present positive angle deviations.

The T axes of events from L1 to L14 are directed to an apparent pole at 136.3°E, 39.9°N, which is placed on the trench-normal axis crossing the peak-slip region (Fig. 5). The depth of the apparent pole is ∼208.0 km. This T-axis focusing is observed at the cross-sections with large slips (L1–L14), while not obvious at the cross-sections with slips less than 7–10 m (L15–L21) (Fig. 4). This apparent pole composes a circular arc with a radius of 697.3 km on the Earth's surface, and a circular arc along the slab surface with a radius of 727.6 km (Fig. 5).

The focusing T-axis directions are consistent with finite fault slip models for the megathrust (Hayes, 2011; Yoshida et al., 2011). The coincident of directions between the T axes of normal-faulting events and coseismic ruptures supports the subsequent postseismic lithospheric deformation following the coseismic rupture. Thus, a comparison between T axes directions and plate convergence directions allows us to infer the properties of coseismic and postseismic lithospheric deformation. The focusing T axes suggest that lithospheric rebound is initiated by the large rupture on the slab surface. The T-axis distribution suggests that the upper lithosphere was deformed radially from a location behind the peak-slip region due to interplate coupling during lithospheric rebound.

9. Slip-dependent earthquake occurrence rates

The earthquake occurrence rates (*b* values) are influenced by asperities, frictional properties, and interface locking along subduction zones (Sobiesiak et al., 2007; Schorlemmer and Wiemer, 2005; Ghosh et al., 2008). Additionally, the crustal deformation causes a change in stress field, which influences the earthquake occurrence rate. Thus, spatial and temporal changes of *b* values present the stress state of the medium (Smith, 1981; Schorlemmer et al., 2005). We investigate the temporal variation

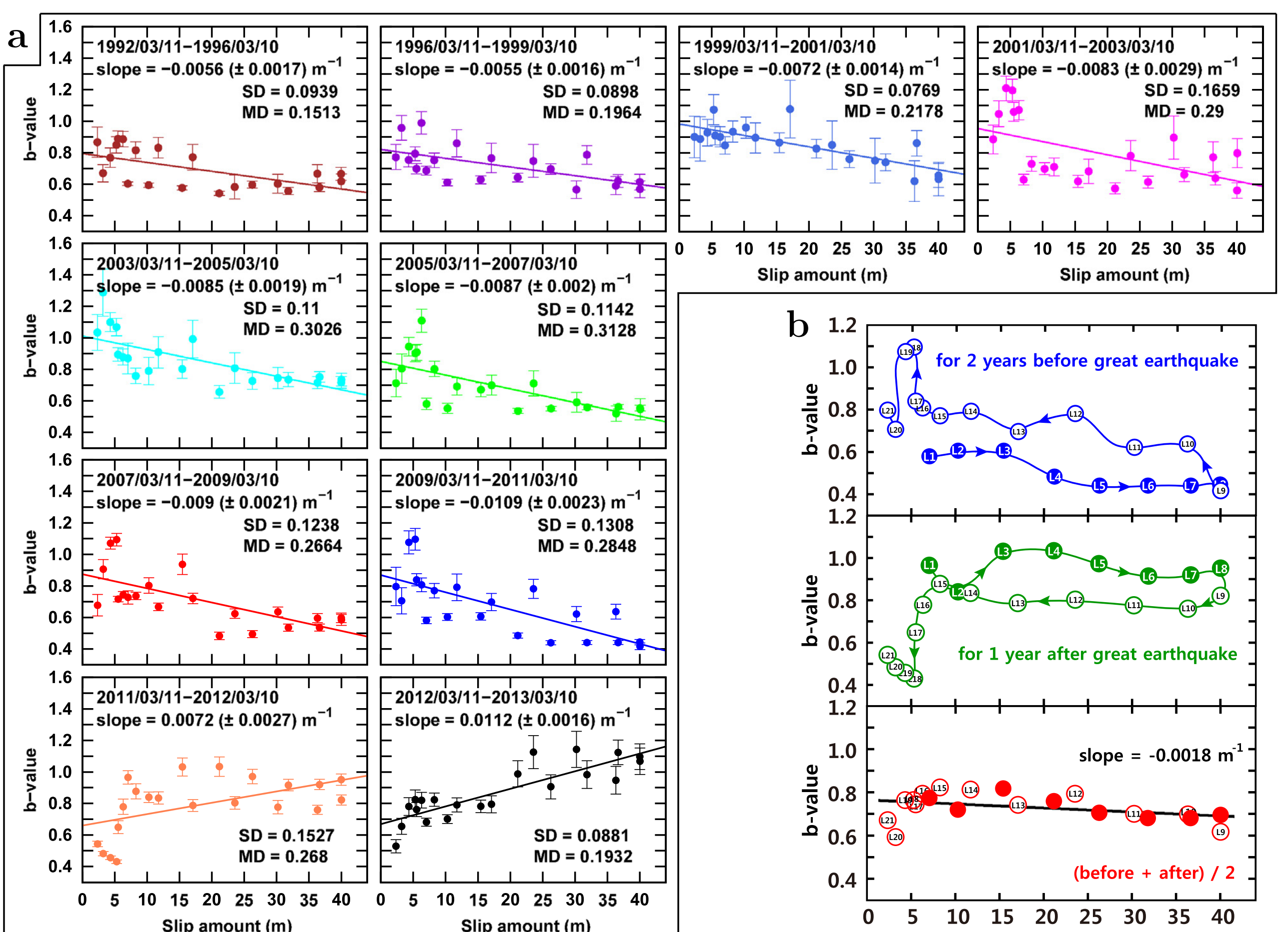

Fig. 8. (a) Variation in *b* values before the Tohoku-Oki earthquake as a function of slip amount for L1 to L21. The slip-dependent *b* values decrease with time until the occurrence of the megathrust. The *b* values increase abruptly after the megathrust. The *b* values before and after the megathrust are anti-correlated. (b) A comparison of average *b* values before and after the megathrust for L1 to L21. The average *b* values are similar among various regions.

of b values in the inner-trench region of the Tohoku-Oki earthquake for cross-sections L1 to L21, which allows us to deduce the upper-crustal response during interplate locking.

Fig. 6 presents b values for the events in zone I of every cross-section from L1 to L21 over 11 March 2001 to 10 March 2003. The average slip amount is also presented in the figure. It is observed that the b values change with the slip amount of forthcoming megathrust. Fig. 7 presents the b value variation with time before and after the megathrust. The b values decrease generally with time in every cross-section, which is consistent with Nanjo et al. (2012). The decrease rates of b values with time are high in large-slip regions, with some exceptions. This observation suggests that the b value may change with slip amount, as well as with various time-dependent factors. Thus, temporal decay rates of b values do not appear to be correlated with the size of forthcoming event. Furthermore, the timing of event occurrence is difficult to estimate from the temporal decay rates of b values.

Fig. 8 (a) presents the b value variations as a function of average slip amount for specified time periods. The b values are low for every time period before the megathrust in the regions with large slip amounts, while they are high in the regions with small slip amounts. Also, the slope of line fitted to the b values of each time period increases with time until the megathrust occurrence. The slope of b values as a function of average slip amount is found to be $-0.0056\ \mathrm{m}^{-1}$ in the period from 1992 to 1996. The slope increases progressively with time, and reaches $-0.0109\ \mathrm{m}^{-1}$ in one year before the Tohoku-Oki earthquake. This observation suggests that the temporal decay rates of b values in large slip regions are larger than those in small slip regions.

After the megathrust (2011/03/11–2012/03/10, 2012/03/11–2013/03/10), the b values generally increased in all regions, particularly in those with large slips (Fig. 8 (a)). Thus, the slope becomes positive after the megathrust: $0.0072\ \mathrm{m}^{-1}$ in the first year after the Tohoku-Oki earthquake and $0.0112\ \mathrm{m}^{-1}$ in the second year. The abrupt increase in b value after the megathrust may be due to interplate decoupling after coseismic rupture (e.g., Nishimura et al., 2004).

It is noteworthy that the correlations between b values and slip amounts observed in this study are much stronger than those in Nanjo et al. (2012). The slip-dependent decrease in b values at every time period appears to be observed at least 20 years before the megathrust. This feature may be because time-dependent factors affecting b values, except slip amount, are activated consistently over the source region.

The b values display a characteristic anti-correlation before and after the megathrust. Thus, the average b values before and after the megathrust are similar, around 0.6–0.8 on the cross-sections (Fig. 8(b)). This feature suggests that the total amount of stress released is comparable over the entire slab interface regardless of the slip amount during the megathrust. In other words, the stress unleased during the locking process is eventually released by megathrust and aftershocks. Thus, the high seismicity in the rupture area after the megathrust can be ascribed to the accumulated preseismic stress in the region. The anti-correlation of the b values before and after the megathrust and the similar average b values also suggest that b values have a strong linear relationship with slip amounts of the forthcoming megathrust.

The slopes for b-value variations as a function of average slip amount are shown in Fig. 9, in which negative slopes clearly increase with time before the megathrust. The slopes then display an abrupt positive increase after the megathrust. The increase in negative slopes with time before the megathrust suggests an interplate locking process that is enhanced with time. Stress is accumulated in the locked region on the slab boundary, causing the decrease in b values. In particular, the b value variation suggests

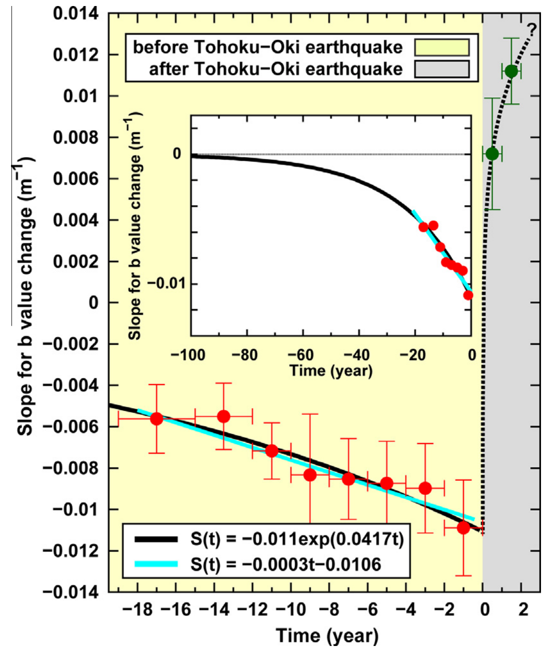

Fig. 9. Variation in slip-dependent b-value change rates, $S(t)$, as a function of time in year t, which is fitted by an exponential function. The slip-dependent b-value change rate increases negatively with time until the occurrence of the megathrust, and increases positively after the megathrust. The average rate of the slip-dependent b-value changes for 22 years in the Tohoku-Oki earthquake region is $-0.0003\ (\pm\ 0.00004)\ \mathrm{m}^{-1}\ \mathrm{yr}^{-1}$.

that the variation in medium properties accelerates with time as time approaches the megathrust.

The slopes for b-value variations before the megathrust display a consistent variation with time, which can be fitted with an exponential function (Fig. 9):

$$S(t) = -0.011\exp(0.0417 \cdot t), \tag{4}$$

where $S(t)$ is the fitting function as a function of lag time in years, t, with respect to the origin time of megathrust. Also, the average variation of the slopes for b value variations can be determined using a linear regression:

$$S(t) = -0.0003t - 0.0106. \tag{5}$$

The observation of region-dependent b value changes with time suggests temporal variation of the medium properties before and after megathrusts. The temporal changes appear to accelerate with time as time approaches the megathrust occurrence. A megathrust occurs when a certain level of stress is accumulated. Thus, the temporal variation in the slopes of b value variations may be a useful precursor of a forthcoming megathrust. The fitted functions may be used for determining the event occurrence time and size of the forthcoming earthquake from $S(t)$ by assuming the distribution of slip amounts of the forthcoming event and a consistent stress release mechanism.

10. Discussion and conclusions

The seismicity properties before and after the three megathrusts with magnitudes greater than or equal to 8.8 since 2000 have been investigated. The seismicity increased significantly after the megathrusts, accompanying changes in the composition of faulting types. Normal-faulting events are concentrated in the large-slip regions at shallow depths. The number of normal-faulting events is proportional to slip amount and vertical surface displacement. This proportionality is dependent on the spatial distribution of slow slip events, local geology, and lithospheric response to dynamic stress changes. Thrustal earthquakes are observed to be clustered at the down-dip margin of the rupture plane, where unleased compressional stress is accumulated.

In the Tohoku-Oki earthquake region, the directions of tensional axes for normal-faulting earthquakes display systematic deviations from the opposite direction of the ambient compressional stress field. The angle deviations increase with trench-parallel distance from the peak-slip region. The tensional axes appear to focus at a location in the forearc region between Tohoku and the peak-slip regions. The observation suggests that the lithosphere rebounded radially from the apparent focus of the tensional axes after the megathrust.

The earthquake occurrence rates (*b* value) decrease with time as a function of slip amount before the Tohoku-Oki earthquake. The slip-dependent *b*-value decreases accelerate with time. The decreasing *b* values suggests that interplate locking on the slab surface is enhanced with time and accumulated stress. The megathrust occurred when the accumulated stress reached the critical level. Aftershocks were increased after the megathrust, yielding an abrupt increase in the earthquake occurrence rates. The average values of *b* values before and after the megathrust are similar among various regions with different slip amounts, which suggests that the cumulative amount of stress released is similar over the entire source region, regardless of the slip amounts.

The temporal change in slip-dependent *b* values is fitted well with an exponential function, which suggests that the temporal change of slip-dependent *b* values may allow us to predict the occurrence time of a forthcoming megathrust. Considering the level of errors in the estimation of *b* values, the slip-dependent *b* value change is identifiable at least several decades before a megathrust. The temporal change rate of slip-dependent *b* value variation allows us to estimate the amount of stress accumulated in the locked zone, enabling us to predict the size of the earthquake. Moreover, the occurrence timing of a forthcoming event may be predictable when the size of earthquake is assumed.

Acknowledgements

We are grateful to Drs. Suito Hisashi and Marcos Moreno for the digital surface displacement models of the Tohoku-Oki and Maule earthquakes. We thank the editor, Professor Vernon Cormier, and the anonymous reviewers for their valuable comments that improved the paper. This work was supported by the Korea Meteorological Administration Research and Development Program under Grant CATER 2012–8050.

References

Abercrombie, R.E., Mori, J., 1996. Occurrence patterns of foreshocks to large earthquakes in the western United States. Nature 381, 303–307.
Aki, K., Richards, P.G., 1980. Quantitative Seismology. Theory and Methods, vol. 1. W.H. Freeman and Company, San Francisco.
Ammon, C.J., Ji, C., Thio, H.-K., Robinson, D., Ni, S., Hjorleifsdottir, V., Kanamori, H., Lay, T., Das, S., Helmberger, D., Ichinose, G., Polet, J., Wald, D., 2005. Rupture process of the 2004 Sumatra-Andaman earthquake. Science 308, 1133–1139.
Angermann, D., Klotz, J., Reigber, C., 1999. Space-geodetic estimation of the Nazca-South, America Euler vector. Earth Planet. Sci. Lett. 171, 329–334.
Apel, E.V., Bürgmann, R., Steblov, G., Vasilenko, N., King, R., Prytkov, A., 2006. Independent active microplate tectonics of northeast Asia from GPS velocities and block modeling. Geophys. Res. Lett. 33, L11303. http://dx.doi.org/10.1029/2006GL026077.
Arabelos, D., Asteriadis, G., Contadakis, M., Zioutas, G., Xu, D., Zhang, C., Zheng, B., 2001. The use of an outlier detecting method in time series of continuous daily measurements of underground water level and temperature in earthquake prediction investigation. Tectonophysics 338, 315–323.
Asano, Y., Saito, T., Ito, Y., Shiomi, K., Hirose, H., Matsumoto, T., Aoi, S., Hori, S., Sekiguchi, S., 2011. Spatial distribution and focal mechanisms of aftershocks of the 2011 off the Pacific coast of Tohoku earthquake. Earth Planet. Space 63, 669–673.
Beavan, J., Wang, X., Holden, C., Wilson, K., Power, W., Prasetya, G., Bevis, M., Kautoke, R., 2010. Near-simultaneous great earthquakes at Tongan megathrust and outer rise in September 2009. Nature 466, 959–963.
Bird, P., 2003. An updated digital model of plate boundaries. Geochem. Geophys. Geosyst. 4 (3), 1027. http://dx.doi.org/10.1029/2001GC000252.
Conin, M., Henry, P., Godard, V., Bourlange, S., 2012. Splay fault slip in a subduction margin, a new model of evolution. Earth Planet. Sci. Lett. 341-344, 170–175.
Cubas, N., Avouac, J.P., Leroy, Y.M., Pons, A., 2013. Low friction along the high slip patch of the 2011 Mw 9.0 Tohoku-Oki earthquake required from the wedge structure and extensional splay faults. Geophys. Res. Lett. 40, 4231–4237.
Delouis, B., Nocquet, J.-M., Vallée, M., 2010. Slip distribution of the February 27, 2010 Mw = 8.8 Maule earthquake, central Chile, from static and high-rate GPS, InSAR, and broadband teleseismic data. Geophys. Res. Lett. 37, L17305. http://dx.doi.org/10.1029/2010GL043899.
Enescu, B., Ito, K., 2001. Some premonitory phenomena of the 1995 Hyogo-Ken Nanbu (Kobe) earthquake: seismicity, *b*-value and fractal dimension. Tectonophysics 338, 297–314.
Frohlich, C., 1992. Triangle diagrams: ternary graphs to display similarity and diversity of earthquake focal mechanisms. Phys. Earth Planet. Inter. 75 (1-3), 193–198.
Gasperini, P., Vannucci, G., 2003. FPSPACK: a package of FORTRAN subroutines to manage earthquake focal mechanism data. Comput. Geosci. 29, 893–901.
Ghosh, A., Newman, A.V., Thomas, A.M., Farmer, G.T., 2008. Interface locking along the subduction megathrust from b-value mapping near Nicoya Peninsula, Costa Rica. Geophys. Res. Lett. 35, L01301. http://dx.doi.org/10.1029/2007GL031617.
Hayes, G.P., 2010. The Feb 27, 2010 Mw 8.8 Maule, Chile earthquake, http://earthquake.usgs.gov/earthquakes/eqinthenews/2010/us2010tfan/finite_fault.php.
Hayes, G.P., 2011. Rapid source characterization of the 2011 Mw 9.0 off the Pacific coast of Tohoku earthquake. Earth Planets Space 63, 529–534.
Hayes, G.P., Wald, D.J., Johnson, R.L., 2012. Slab1.0: a three-dimensional model of global subduction zone geometries. J. Geophys. Res. 117, B01302. http://dx.doi.org/10.1029/2011JB008524.
Heki, K., Miyazaki, S., Tsuji, H., 1997. Silent fault slip following an interplate thrust earthquake at the Japan Trench. Nature 386, 595–597.
Hoechner, A., Babeyko, A.Y., Sobolev, S.V., 2008. Enhanced GPS inversion technique applied to the 2004 Sumatra earthquake and tsunami. Geophys. Res. Lett. 35, L08310. http://dx.doi.org/10.1029/2007Gl033133.
Ide, S., 2013. The proportionality between relative plate velocity and seismicity in subduction zones. Nat. Geosci. 6, 780–784.
Ito, Y., Hino, R., Kido, M., Fujimoto, H., Osada, Y., Inazu, D., Ohta, Y., Iinuma, T., Ohzono, M., Miura, S., Mishina, M., Suzuki, K., Tsuji, T., Ashi, J., 2013. Episodic slow slip events in the Japan subduction zone before the 2011 Tohoku-Oki earthquake. Tectonophysics 600, 14–26.
Ji, C., 2005. Magnitude 9.1 Off the West Coast of Northern Sumatra, http://neic.usgs.gov/neis/eq_depot/2004/eq_041226/neic_slav_ff.html.
Kanamori, H., 1972. Mechanism of tsunami earthquakes. Phys. Earth Planet. In. 6, 346–359.
Kanamori, H., 1986. Rupture process of subduction-zone earthquakes. Ann. Rev. Earth Planet. Sci. 14, 293–322.
Keliang, Z., Jin, M., 2011. Numerical simulation of co-seismic deformation of 2011 Japan Mw9. 0 earthquake. Geodesy Geodyn. 2 (3), 16–23.
Lay, T., Astiz, L., Kanamori, H., Christensen, D.H., 1989. Temporal variation of large intraplate earthquakes in coupled subduction zones. Phys. Earth Planet. Inter. 54, 258–312.
Lay, T., Ammon, C.J., Kanamori, H., Koper, K.D., Sufri, O., Hutko, A.R., 2010. Teleseismic inversion for rupture process of the 27 February 2010 Chile (Mw 8.8) earthquake. Geophys. Res. Lett. 37, L13301. http://dx.doi.org/10.1029/2010GL043379.
Lin, W., Conin, M., Moore, J.C., Chester, F.M., Nakamura, Y., Mori, J.J., Anderson, L., Brodsky, E.E., Eguchi, N., and Expedition 343 Scientists, 2013. Stress state in the largest displacement area of the 2011 Tohoku-Oki earthquake, Science, 339, 687–690.
Lu, J., Qian, F., Zhao, Y., 1999. Sensitivity analysis of the Schlumberger monitoring array: application to changes of resistivity prior to the 1976 earthquake in Tangshan, China. Tectonophysics 307, 397–405.
McKenzie, D., Jackson, J., 2012. Tsunami earthquake generation by the release of gravitational potential energy. Earth Planet. Sci. Lett. 345-348, 1–8.
Mikada, H., Mitsuzawa, K., Matsumoto, H., Watanabe, T., Morita, S., Otsuka, R., Sugioka, H., Baba, T., Araki, E., Suyehiro, K., 2006. New discoveries in dynamics of an M8 earthquake-phenomena and their implications from the 2003 Tokachi-oki earthquake using a long term monitoring cabled observatory. Tectonophysics 426, 95–105.
Minoura, K., Imamura, F., Sugawara, D., Kono, Y., Iwashita, T., 2001. The 869 Jōgan tsunami deposit and recurrence interval of large-scale tsunami on the Pacific coast of northeast Japan. J. Nat. Disaster Sci. 23 (2), 83–88.
Moreno, M., Rosenau, M., Oncken, O., 2010. 2010 Maule earthquake slip correlates with pre-seismic locking of Andean subduction zone. Nature 467, 198–202.
Moreno, M., Melnick, D., Rosenau, M., Baez, J., Klotz, J., Oncken, O., Tassara, A., Chen, J., Bataille, K., Bevis, M., Socquet, A., Bolte, J., Vigny, C., Brooks, B., Ryder, I., Grund, V., Smalley, B., Carrizo, D., Bartsch, M., Hase, H., 2012. Toward understanding tectonic control on the Mw 8.8 2010 Maule Chile earthquake. Earth Planet. Sci. Lett. 321-322, 152–165.
Nanjo, K.Z., Hirata, N., Obara, K., Kasahara, K., 2012. Decade-scale decrease in b value prior to the M9-class 2011 Tohoku and 2004 Sumatra quakes. Geophys. Res. Lett. 39, L20304. http://dx.doi.org/10.1029/2012GL052997.

Narteau, C., Byrdina, S., Shebalin, P., Schorlemmer, D., 2009. Common dependence on stress for the two fundamental laws of statistical seismology. Nature 462, 642–645.

Newcomb, K.R., McCann, W.R., 1987. Seismic history and seismotectonics of the Sunda arc. J. Geophys. Res. 92 (B1), 421–439.

Nishimura, T., Hirasawa, T., Miyazaki, S., Sagiya, T., Tada, T., Miura, S., Tanaka, K., 2004. Temporal change of interplate coupling in northeastern Japan during 1995-2002 estimated from continuous GPS observations. Geophys. J. Int. 157, 901–916.

Nuannin, P., Kulhánek, O., Persson, L., 2005. Spatial and temporal b value anomalies preceding the devastating off coast of NW Sumatra earthquake of December 26, 2004. Geophys. Res. Lett. 32, L11307. http://dx.doi.org/10.1029/2005Gl022679.

Nuannin, P., Kulhánek, O., Persson, L., 2012. Variations of *b*-values preceding large earthquakes in the Andaman-Sumatra subduction zone. J. Asian Earth Sci. 61, 237–242.

Obana, K., Fujie, G., Takahashi, T., Yamamoto, Y., Nakamura, Y., Kodaira, S., Takahashi, N., Kaneda, Y., Shinohara, M., 2012. Normal-faulting earthquakes beneath the outer slope of the Japan Trench after the 2011 Tohoku earthquake: Implications for the stress regime in the incoming Pacific plate. Geophys. Res. Lett. 39, L00G24. http://dx.doi.org/10.1029/2011GL050399.

Ogata, Y., Katsura, K., 1993. Analysis of temporal and spatial heterogeneity of magninute frequency distribution inferred from earthquake catalogues. Geophys. J. Int. 113, 727–738.

Ozawa, S., Nishimura, T., Suito, H., Kobayashi, T., Tobita, M., Imakiire, T., 2011. Coseismic and postseismic slip of the 2011 magnitude-9 Tohoku-Oki earthquake. Nature 475, 373–376.

Pollitz, F.F., Brooks, B., Tong, X., Bevis, M.G., Foster, J.H., Bürgmann, R., Smalley Jr., R., Vigny, C., Socquet, A., Ruegg, J.-C., Campos, J., Barrientos, S., Parra, H., Soto, J.C.B., Cimbaro, S., Blanco, M., 2011. Coseismic slip distribution of the February 27, 2010 Mw 8.8 Maule, Chile earthquake. Geophys. Res. Lett. 38, L09309. http://dx.doi.org/10.1029/2011GL047065.

Schorlemmer, D., Wiemer, S., 2005. Microseismicity data forecast rupture area. Nature 434, 1086.

Schorlemmer, D., Wiemer, S., Wyss, M., 2005. Variation in earthquake-size distribution across different stress regimes. Nature 437, 539–542.

Seno, T., Sakurai, T., 1996. Can the Okhostsk plate be discriminated from the North American plate? J. Geophys. Res. 101 (B5), 11305–11315.

Shinohara, M., Machida, Y., Yamada, T., Nakahigashi, K., Shinbo, T., Mochizuki, K., Murai, Y., Hino, R., Ito, Y., Sato, T., Shiobara, H., Uehira, K., Yakiwara, H., Obana, K., Takahashi, N., Kodaira, S., Hirata, K., Tsushima, H., Iwasaki, T., 2012. Precise aftershock distribution of the 2011 off the Pacific coast of Tohoku earthquake revealed by an ocean-bottom seismometer network. Earth Planets Space 64, 1137–1148.

Smith, W.D., 1981. The b-value as an earthquake precursor. Nature 289, 136–139.

Sobiesiak, M., Meyer, U., Schmidt, S., Götze, H.-J., Krawczyk, C.M., 2007. Asperity generating upper crustal sources revealed by *b* value and isostatic residual anomaly grids in the area of Antofagasta, Chile. J. Geophys. Res. 112, B12308. http://dx.doi.org/10.1029/2006JB004796.

Song, T.-R.A., Simons, M., 2003. Large trench-parallel gravity variations predict seismogenic behavior in subduction zones. Science 301, 630–632.

Stein, S., Wysession, M., 2003. An Introduction to Seismology, Earthquakes, and Earth Structure. Blackwell, Oxford, U.K.

Tanioka, Y., Yudhicara, Kususose, T., Kathiroli, S., Nishimura, Y., Iwasaki, S.-I., Satake, K., 2006. Rupture process of the 2004 great Sumatra-Andaman earthquake estimated from tsunami waveforms. Earth Planets Space 58, 203–209.

Vigny, C., Simons, W.J.F., Abu, S., Bamphenyu, R., Satirapod, C., Choosakul, N., Subarya, C., Socquet, A., Omar, K., Abidin, H.Z., Ambrosius, B.A.C., 2005. Insight into the 2004 Sumatra-Andaman earthquake from GPS measurements in southeast Asia. Nature 436, 201–206.

Wesnousky, S.G., 1994. The Gutenberg-Richter or characteristic earthquake distribution, which is it? Bull. Seismol. Soc. Am. 84 (6), 1940–1959.

Wiemer, S., Wyss, M., 2000. Minimum magnitude of completeness in earthquake catalogs: examples from Alaska, the Western United States, and Japan. Bull. Seismol. Soc. Am. 90 (4), 859–869.

Woessner, J., Wiemer, S., 2005. Assessing the quality of earthquake catalogues: estimating the magnitude of completeness and its uncertainty. Bull. Seismol. Soc. Am. 95 (2), 684–698.

Wyss, M., Martirosyan, A.H., 1998. Seismic quiescence before the M7, 1988, Spitak earthquake, Armenia. Geophys. J. Int. 134, 329–340.

Yagi, Y., Fukahata, Y., 2011. Rupture process of the 2011 Tohoku-oki earthquake and absolute elastic strain release. Geophys. Res. Lett. 38 (19), L19307. http://dx.doi.org/10.1029/2011GL048701.

Yoshida, K., Miyakoshi, K., Irikura, K., 2011. Source process of the 2011 off the Pacific coast of Tohoku Earthquake inferred from waveform inversion with long-period strong-motion records. Earth Planets Space 63, 577–582.